Nuclear Physics B82 (1974) 282–312. North-Holland Publishing Company

HIGH-ENERGY PRODUCTION AND DECAY OF VECTOR AND TENSOR MESONS

A.C. IRVING and C. MICHAEL
CERN, Geneva

Received 18 March 1974

Abstract: The available charge-exchange data for $\pi N \to \rho N$, $\pi N \to \omega N$ and $\rho - \omega$ interference effects in the momentum range 6–17 GeV/c are analyzed. Duality considerations are used to constrain as much as possible the exchanged Regge poles and also to relate their contributions to those made by the same Regge exchanges in $\pi N \to f^0 N$ and $\pi N \to A_2 N$. Combined with an empirical investigation of the Regge cut contributions, this allows a simultaneous description of vector and tensor meson production. The resulting amplitudes are used to predict interference effects in the common $K\bar{K}$ decay channel of f^0 and A_2. Other predictions include $K^*(1420)$ and $\overline{K}^*(1420)$ production, and many polarization effects.

1. Introduction

With the increasing abundance of data on resonance production processes, it has become possible to investigate closely the structure of the exchange amplitudes. The usefulness of a description in terms of t-channel Regge-pole exchange with s-channel modifications (cuts or absorption) has been confirmed [1]. The simplest approach would be to restrict the Regge-pole exchanges by dual constraints (exchange degeneracy, etc.), factorization and SU(3), and to restrict the cuts to amplitudes of zero over-all helicity flip n. We shall pursue such a simple approach with its considerable predictive power and shall try to identify any possible indications for relaxing the constraints.

The advent of spectrometer data on the production of higher mass resonances will introduce a further exciting line of investigation. Higher mass (and spin) resonances are produced in reactions that have the same exchange quantum numbers as their basic counterparts (e.g. $\pi N \to f^0 N$ or $\pi N \to gN$ relative to $\pi N \to \rho N$). It is thus a challenge to existing theories to account for the production mechanisms of such states. Dual theories, both more generally through local duality applied to finite mass sum rules [2, 3], and more specifically from the explicit dual model vertex structure [4], have characteristic predictions to make. We use these ideas to make a preliminary study of tensor meson production based on the knowledge of vector meson production.

In sect. 2, we discuss the available data (6–17 GeV/c) on $\pi N \to \rho N$ and $\pi N \to \omega N$

and establish models for the exchange contributions. Interference effects between ρ and ω production amplitudes are observable as a result of ρ–ω electromagnetic mixing in the $\pi\pi$ decay, and also from comparison with the SU(3) related processes $KN \to K^*N$ and $\bar{K}N \to \bar{K}^*N$. Our decomposition of the ρ and ω production amplitudes into exchange contributions is consistent with data on such interference effects and, in sect. 3, we discuss predictions for nucleon polarization observables which will provide further insight into the amplitude structure.

Armed with a model for vector meson production, in sect. 4, we use the dual model expectations as a guide in discussing the charge-exchange tensor meson production reactions $\pi N \to f^0 N$ and $\pi N \to A_2 N$. The available data are well described. As an additional sensitive test, we present, in sect. 5, predictions for the interference effects to be seen in the $K\bar{K}$ decay channel which is common to A_2 and f^0. Likewise $K^*(1420)$ and $\bar{K}^*(1420)$ production are discussed.

Conclusions are presented in sect. 6.

2. Vector-meson production

Spin-1 meson production on nucleons involves six helicity amplitudes which are connected to the observable density matrix elements as follows (see also appendix A)

$$\sigma_0^{\mathrm{u}} = \rho_{00}\mathrm{d}\sigma/\mathrm{d}t = |P^0_{++}|^2 + |P^0_{+-}|^2 = |P_0|^2 ,$$

$$\sigma_-^{\mathrm{u}} = (\rho_{11} - \rho_{1-1})\mathrm{d}\sigma/\mathrm{d}t = |P^-_{++}|^2 + |P^-_{+-}|^2 = |P_-|^2 ,$$

$$\sigma^{\mathrm{n}} = (\rho_{11} + \rho_{1-1})\mathrm{d}\sigma/\mathrm{d}t = |P^+_{++}|^2 + |P^+_{+-}|^2 = |P_+|^2 ,$$

$$\sqrt{2}\ \mathrm{Re}\,\rho_{10}\mathrm{d}\sigma/\mathrm{d}t = \mathrm{Re}\,(P^-_{++}P^{0*}_{++} + P^-_{+-}P^{0*}_{+-}) , \tag{2.1}$$

where

$$P^{\pm}_{\lambda\nu} = \sqrt{\tfrac{1}{2}}(H^{+1}_{\lambda\nu} \pm H^{-1}_{\lambda\nu}) .$$

Allowance [5, 6] can be made for the presence of S-wave background under the P-wave vector meson signal. Thus the modulus of $\lambda = 0$ and 1 unnatural parity exchange contributions (σ_0^{u} and σ_-^{u}), their interference $\mathrm{Re}\,\rho_{10}$, and the natural parity exchange contribution σ^{n} can be separated. Further separation of the amplitudes requires, at present, assumptions about the nature of the exchange contributions. In principle, however, polarization observables will allow [7] a determination of the moduli and relative phases of each amplitude. In practice, an incomplete set of polarization measurements (e.g. polarized target without recoil polarization analysis) will allow stringent tests of the assumptions to be made about exchange amplitudes.

2.1. $\pi^- p \to \rho^0 n$

The quantum numbers allowed in the t-channel are such that only a restricted set of Regge-pole exchanges should contribute. These are discussed in turn.

2.1.1. π exchange. We treat the pion as a Regge pole with a slope just like any other particle exchange. The proximity of the $J = 0$ π-pole to the physical region implies that the Regge description is essentially the same for small t as a one-particle exchange expression. From consideration of the Chew-Frautschi plot for unnatural parity mesons we expect

$$\alpha_\pi(t) = \alpha'(t - \mu^2) = 0.82(t - \mu^2) ,$$

where μ is the pion mass and the value of α' comes from assuming linear exchange degenerate trajectories $\pi - \mathrm{H}$ or $\eta - \mathrm{B}$. The $J = 0$ π-pole couples only to $\lambda_t = 0$ ρ mesons (λ_s and λ_t refer respectively to s- and t-channel helicity frames). Away from the nonsense zero at $\alpha_\pi(t) = 0$, however, a Regge π trajectory should couple to $\lambda_t \neq 0$ and this contribution could become significant for $-t \sim 0.5$ GeV^2. A simple estimate of a reasonable strength for such a $\lambda_t = 1$ contribution comes [4] from the structure of the dual resonance model vertex. This yields, for the t-channel helicity frame,

$$\frac{\pi_-^t}{\pi_0^t} = \frac{2\sqrt{-t}(\mu^2 - t)}{m(m^2 - \mu^2 - 3t)} . \tag{2.2}$$

where $m = m_\rho$ and π_-^t vanishes at $t = \mu^2$ as discussed previously. In terms of s-channel helicity amplitudes, this takes on the simple form [4]

$$\frac{\pi_-^s}{\pi_0^s} = \frac{2\sqrt{-t}}{m} . \tag{2.3}$$

The more popular assumption of taking $\pi_-^t = 0$ leads to $\pi_-^s/\pi_0^s = 2\sqrt{-t}\, m/(m^2 + t - \mu^2)$, which is significantly different in the neighbourhood of the zero of π_0^s at $-t = m^2 - \mu^2$.

At the nucleon vertex, the π Regge trajectory couples to the helicity flip only. Thus its contribution to P_{+-}^0 and P_{+-}^- will be in the above ratio. A simple parametrization for the $\lambda_s = 0$ amplitude valid up to moderate t-values is

$$\pi_{+-}^0 = \frac{\sqrt{-t}\, g_\pi}{\mu^2 - t} \frac{m}{\sqrt{m^2 - 4\mu^2}} \mathrm{e}^{b_\pi t} \mathrm{e}^{-\frac{1}{2} i\pi\alpha_\pi(t)} \left(\frac{p_\mathrm{L}}{p_0}\right)^{\alpha_\pi(t)-1} , \tag{2.4}$$

where p_L is lab momentum and p_0 is chosen for convenience as 17.2 GeV/c. A constant factor has been included to assist the identification of g_π with the residue of the t-channel π exchange pole (appendix A).

2.1.2. A_2 exchange. The A_2 Regge pole may couple to the amplitudes P^+_{+-} and P^+_{++}. We expect a trajectory

$$\alpha_A(t) = 0.5 + \alpha' t.$$

The ratio of flip to non-flip coupling at the nucleon vertex may be related by factorization to that found in $\pi N \to \eta N$ and KN charge exchange. In terms of the invariant coupling A' and A for such processes we have A_2 exchange ratios

$$\frac{A^+_{+-}}{A^+_{++}} = \frac{-\sqrt{-t}}{2m_N}\frac{A}{A'} = \frac{\sqrt{-t}}{r}, \tag{2.5}$$

and thus $r \sim 0.5$ for the vector dominance expectation [8] $A/A' \sim -3.7$, while $r \sim 0.25$ for the empirical values of $A/A' \sim -8$ found in effective pole fits to $0^-\tfrac{1}{2}^+ \to 0^-\tfrac{1}{2}^+$ processes [9]. A parametrization for the s and t dependence of the A_2 exchange pole contribution is

$$A^+_{+-} = -t' g_A e^{b_A t} e^{-\frac{1}{2}i\pi\alpha_A(t)} \left(\frac{p_L}{p_0}\right)^{\alpha_A(t)-1}. \tag{2.6}$$

2.1.3. Cut contribution. The contributions from the π and A_2 Regge poles have long been known [10] to be insufficient to describe the data on $\pi N \to \rho N$. In particular, the data are non-zero in the forward direction, while the Regge contributions all vanish as $t' \to 0$. It is traditional [10] to incorporate a background, Regge cut, or absorptive correction C which does not vanish as $t' \to 0$. This can be motivated from s-channel Born term or dual arguments, via absorption of low partial waves, or from a π-pomeron Regge cut. Our interest lies in an empirical description of the data, however, so that we shall be content with a parametrization of the cut C. The simplest assumption is that C only contributes to the s-channel helicity non-flip amplitude H^1_{+-}. This leads to equal amounts of cut in P^-_{+-} and P^+_{+-}. The phase and energy dependence of C may be obtained from the experimental data and some theoretical assumptions. Since Re ρ_{10} experimentally [6] has its extremum value relative to P_0 and P_-, this implies that P_0 and P_- have the same phase (phase coherence). Thus the phase of C and of the π exchange contributions must be similar. Consideration of their interference in P_+ also leads to constraints [5] on their relative phase as a function of t. A compromise, which also has the virtue of being the naive absorption model result, is to take the phase from an effective trajectory

$$\alpha_C(t) = 0 + \tfrac{1}{2}\alpha' t\,.$$

The energy dependence of the cut contribution is model-dependent – as a simple approximation we take the energy dependence to be given by the same effective trajectory as the phase. Thus the cut is approximated for convenience by an effective (non-factorizing) pole with the above trajectory. Thus our parametrization is

$$C^{+}_{+-} = C^{-}_{+-} = g_C e^{b_C t} e^{-\frac{1}{2} i\pi\alpha_C(t)} \left(\frac{p_L}{p_0}\right)^{\alpha_C(t)-1} . \tag{2.7}$$

2.1.4. Our model. Our combination of π and A_2 pole exchange and effective cut C differs from that of Estabrooks et al. [11] only in details: the $\lambda_t = 1$ π-exchange coupling and the A_2 nucleon non-flip couplings are retained. A further possible contribution – with A_1 quantum number exchange – will be reconsidered subsequently. Thus we have, in the s-channel helicity frame

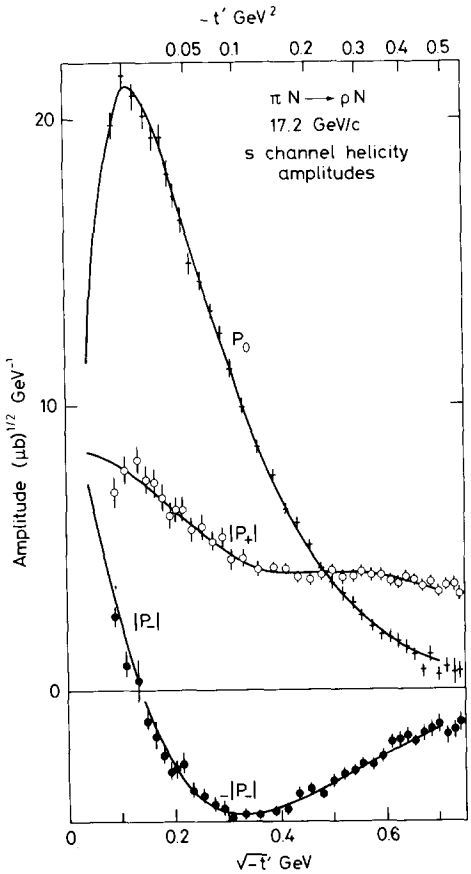

Fig. 1. The moduli of the production amplitudes for $\pi^- p \to \rho^0 n$ at 17.2 GeV/c. The points are the s-channel helicity amplitudes of ref. [12] extracted from the data of ref. [13] and the curves are the fit of the model described in the text. For clarity, $\pm|P_{-}|$ is plotted to exhibit the 180° phase change of P^{-}_{+-} near $\sqrt{-t'} = 0.15$ GeV.

Table 1
Parameters for the models defined in the text in subsect. 2.1 ($\pi^- p \to \rho^0 n$), subsect. 2.2 ($\pi^- p \to \omega^0 n$) and subsect. 4.1 ($\pi^- p \to f^0 n$) [Quantities in square brackets were not varied in the fits; the normalization of g_π is calculated in appendix A.]

$\pi N \to \rho N$

g_π ($\sqrt{\mu b}$)	g_A/g_π (GeV^{-3})	g_C/g_π (GeV^{-1})	b_π (GeV^{-2})	b_A (GeV^{-2})	b_C (GeV^{-2})	r (GeV)
[6.0]	5.17	−1.42	4.51	3.24	6.45	[0.5]

$\pi N \to \omega N$

g_B ($\sqrt{\mu b}$)	g_ρ/g_A	g_Z/g_B (GeV)	C_B/g_B (GeV^{-1})	C_ρ/g_B (GeV^{-1})	b_{C_B} (GeV^{-2})	b_{C_ρ} (GeV^{-2})
6.0	2.0	0.54	−0.20	−0.048	0.97	[$= b_{C_B}$]

$\pi N \to f^0 N$

g_π ($\sqrt{\mu b}$)	g_A/g_π (GeV^{-3})	g_C/g_π (GeV^{-1})	g_{C_2}/g_π (GeV^{-2})	b_π (GeV^{-2})	b_A (GeV^{-2})	b_C (GeV^{-2})
[8.4]	1.35	−0.84	−0.575	[4.51]	[3.24]	3.89

$$P^0_{+-} = \pi^0_{+-} \quad , \quad P^0_{++} = 0,$$

$$P^-_{+-} = \left(\frac{\pi^s_-}{\pi^s_0}\right)\pi^0_{+-} + C_{+-} \quad , \quad P^-_{++} = 0,$$

$$P^+_{+-} = A^+_{+-} + C_{+-} \quad , \quad P^+_{++} = A^+_{++} \, . \tag{2.8}$$

The moduli of P_0, P_- and P_+ obtained [11,12] from an analysis of the 17.2 GeV/c $\pi^- p \to \pi^+\pi^- n$ data [13] determine the parameters introduced above. The normalization (see appendix A) fixes g_π; b_π is given by the t dependence of P_0; the small t-value of P_+ or P_- yields g_C; the t dependence of P_- constrains b_C and then the shape of P_+ as a function of t is sufficient to determine g_A and b_A. The fit is shown in fig. 1. Parameters are given in table 1.

The energy dependence [11, 14] from 6–17.2 GeV/c is then a stringent cross check on the above determination. The break seen [14] at 4–6 GeV/c in the t dependence of P^s_0 is not accounted for, but the energy dependence out to $t \sim -0.3$ is

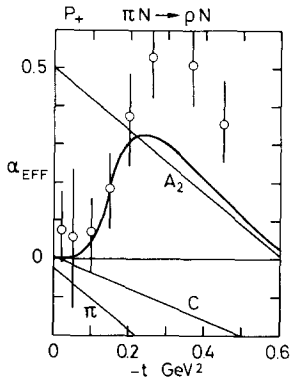

Fig. 2. α_{eff} for $|P_+|^2$ as extracted from the 6 GeV/c [14] and 17.2 GeV/c [13] $\pi^- p \to \rho^0 n$ data in ref. [11] and the prediction of the model (curve). The trajectories assumed for the π, A_2 and cut C contributions are also shown.

satisfactory. Among other possibilities, either a π trajectory of slope $\frac{1}{2}\alpha'$ exactly phase coherent with the cut C, or a small low-lying correction to P_0^S could be tolerated by the data. The energy dependence of P_-^S is in agreement with our model, while the crucial test comes from α_{eff} for P_+ as shown in fig. 2. Here the striking relative increase of natural parity exchange from 6 to 17.2 GeV/c is accounted for by the A_{++}^+ contribution at small t, the $A_{++}^+ - C_{+-}$ destructive interference at moderate t, and the A_2 dominance at larger t. Previous interpretations [15] of $\pi N \to \rho N$ data have had much larger C contributions relative to A_2 at $t \sim -0.3$ to -0.5, so that a much lower value of α_{eff} [close to $\alpha_C(t)$] had been expected.

Our fit with the dual model estimate of π_-^t/π_0^t (eq. (2.2)) is a considerable improvement over taking π_-^t zero when P_0^S would have had a zero at $t \sim -0.5$ and the cut would have [11] a much flatter t dependence ($b_C \sim 1.0$). As a compromise, one can take π_-^t/π_0^t at about 0.5 of the dual vertex value eq. (2.2) when the cut t dependence is very reasonable ($b_C \sim 3.0$). An equally acceptable fit can then be obtained by allowing r to be reduced to 0.25. This compromise description gives a similar value of α_{eff} for P_+, and allows an improved description of the ρ–ω interference phases. Since our present aim is to retain as simple a description as possible in order to extend our analysis to the f^0 production amplitudes, we shall retain the dual model expression for π_-^t/π_0^t of eq. (2.2).

2.2. $\pi N \to \omega N$

We again discuss in turn the various expected exchange contributions. We consider data for the average of $\pi^- p \to \omega n$ and $\pi^+ n \to \omega p$ so that any possible [15] π exchange via ρ–ω electromagnetic mixing will not contribute.

2.2.1. B exchange. The unnatural parity meson spectrum is consistent with π – H and η – B exchange degenerate trajectories split apart by about 0.23. Thus we take the B trajectory as

$$\alpha_B = -0.25 + \alpha' t \ .$$

To allow for the splitting of the trajectories, and relate B to π by exchange degeneracy, we use

$$\frac{B}{\pi} = -\frac{g_B}{g_\pi} \frac{\Gamma(-\alpha_B)}{\Gamma(-\alpha_\pi)} \frac{\sin\frac{1}{2}\pi\alpha_B}{\cos\frac{1}{2}\pi\alpha_\pi} i e^{-\frac{1}{2}i\pi(\alpha_B - \alpha_\pi)} \left(\frac{p_L}{p_0}\right)^{\alpha_B - \alpha_\pi} . \tag{2.9}$$

For strong exchange degeneracy we would have $g_B = g_\pi$; however since $\alpha_\pi \neq \alpha_B$ this comparison depends on p_L. A dual theory would lead to comparison at α's = 1 or $p_L = 1/(2m_N\alpha')$ which yields $g_B = 0.5\, g_\pi$ as an expectation. The helicity couplings of the B exchange are taken from the same model as for the π (eq. (2.3)). The dual vertex factor ensures a pure $\lambda_t = 0$ coupling at $\alpha(t) = 0$ but can also be evaluated at $\alpha(t) = 1$. This yields, at $t = m_B^2$, a ratio of ω production with $\lambda_t = 0$ to all of 0.2. This can be compared directly with the branching fraction of ω with $\lambda_t = 0$ in B decay to $\omega\pi$ which experimentally is quoted [16] as 0.10–0.16. Thus the dual vertex factor successfully reproduces the predominant $\lambda_t = 1$ coupling at $\alpha(t) = 1$, the B mass value.

2.2.2. ρ exchange. This is expected to be exchange degenerate with the A_2 exchange in ρ production and we write $\alpha_\rho(t) = \alpha_A(t)$ and

$$\frac{\rho}{A_2} = \frac{g_\rho}{g_A} i \tan\tfrac{1}{2}\pi\alpha_A \ , \tag{2.10}$$

where $g_\rho = g_A$ for strong exchange degeneracy of the couplings.

2.2.3. Cut C. The B-pole contribution discussed above gives rise to phase coherence for P_- and P_0 and a specific ratio from eq. (2.3). The ρ contribution has a dip at $\alpha_\rho(t) = 0$ in P_+. To take account of possible deviations from these expectations in the data, we introduce a cut in the $n = 0$ amplitude. Guided by the absorption model expectation of cuts mainly 180° out of phase with their respective poles, we parametrize the phase and t dependence of the cut as

$$C^{\pm}_{+-} = (i e^{-\frac{1}{2}i\pi\alpha_B(t)} c_B e^{b_B t} + i e^{-\frac{1}{2}i\pi\alpha_\rho(t)} c_\rho e^{b_\rho t}) \left(\frac{p_L}{p_0}\right)^{\alpha_C(t)-1} . \tag{2.11}$$

As discussed subsequently, data imply $C_B > C_\rho$, so we take $\alpha_C(t) = \alpha_B(t)$ for the energy dependence of the cut.

2.2.4. $J^{PC}I = 2^{-+}1$ exchange. Unnatural parity exchange amplitudes in vector

meson production with nucleon non-flip coupling can only receive contributions from the exchange of axial mesons (A_1 – D nonet) and their $J^{PC} = 2^{-+}$ exchange degenerate partners (no resonance state known). Thus in $\pi N \to \rho N$, A_1 exchange could contribute, but aside from other problems the A_1 contribution has a zero at $\alpha(t) = 0$ (from signature and absense of known $J^{PC} = 0^{-+}$ state), while the π contribution has a pole at $\alpha(t) = 0$. Thus the π is doubly favoured over the A_1 at $\alpha(t) \sim 0$. Conversely, in ω production, the B exchange contribution has a signature zero at $\alpha(t) = 0$, while the Z ($J^P I^G = 2^- 1^+$) exchange contribution would not vanish at $\alpha(t) \sim 0$ and could be relatively important. The only clue for the helicity coupling of Z exchange at the meson vertex comes from the ratio of $A_1 \to \rho(\lambda) + \pi$ with $\lambda = 0$ and 1 in models [17]. This leads to a dominant $\lambda_t = 0$ coupling and for simplicity we use eq. (2.3) to give the s-channel Z^-_{++} to Z^0_{++} coupling ratio. For the t dependence of Z exchange, we make the economical assumption that all the unnatural parity exchanges have similar slopes which leads to

$$\frac{Z_{++}}{B_{+-}} = \frac{g_Z/g_B}{\sqrt{-t'}} \frac{\cos\frac{1}{2}i\pi\alpha_Z}{\sin\frac{1}{2}i\pi\alpha_B} \frac{\Gamma(1-\alpha_Z)}{\Gamma(-\alpha_B)} \left(\frac{p_L}{p_0}\right)^{\alpha_Z - \alpha_B}, \tag{2.12}$$

where g_Z controls the strength (sign unknown) and α_Z is taken as $0 + \alpha' t$.

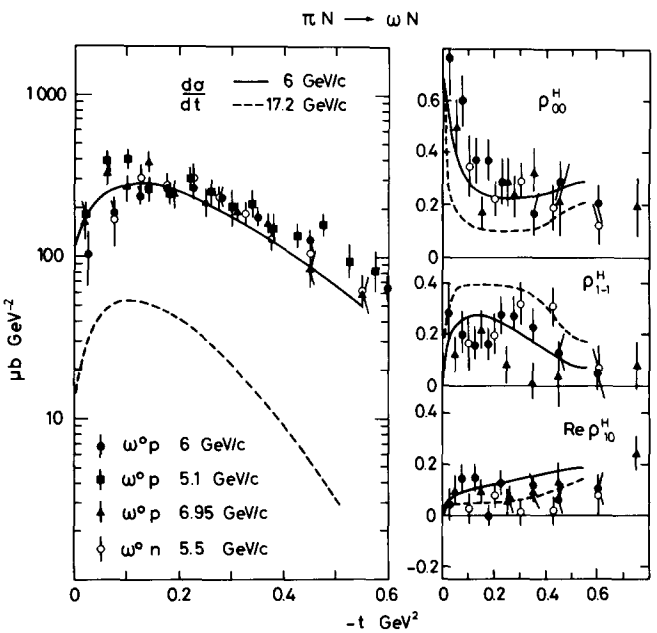

Fig. 3. The data [18, 19] and model fit to $\pi N \to \omega N$ cross section and s-channel density matrix elements at 6 GeV/c. The cross-section data at 5.5, 6.95 and 5.1 GeV/c have been scaled by 0.82, 1.38 and 0.70, respectively [i.e. by $(p_L/6)^{-2.25}$] to an effective momentum of 6 GeV/c. The model prediction for $\pi N \to \omega N$ at 17.2 GeV/c is shown by dotted curves.

2.2.5. Our model. In summary the contributions considered are

$$P^0_{+-} = B^0_{+-}\,, \qquad P^0_{++} = Z^0_{++}\,,$$

$$P^-_{+-} = B^-_{+-} + C^-_{+-}\,, \qquad P^-_{++} = Z^-_{++}\,,$$

$$P^+_{+-} = \rho^+_{+-} + C^+_{+-}\,, \qquad P^+_{++} = \rho^+_{++}\,. \tag{2.13}$$

Insufficient data on $\pi N \to \omega N$ exist to extract a reliable energy dependence of the different components. Thus we consider data [18, 19] in the region of 6 GeV/c, where it is best measured, and attempt to describe it with the above contributions linked to the previous model for ρ production. Some information from ρ–ω interference phases is also anticipated.

Setting $g_Z = 0$, a considerable breaking of exchange degenerary for B is necessary (three times expectation) and the large experimental value of ρ_{00} at small t is not reproduced. The latter can be achieved readily by including a Z exchange contribution. The parameters of a satisfactory description of the data (see fig. 3) are shown in

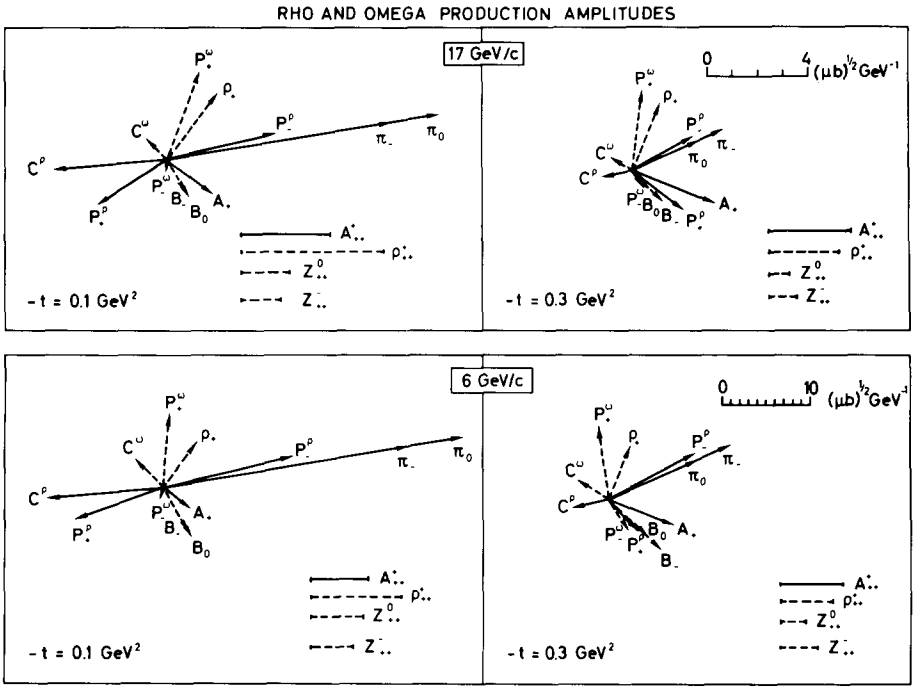

Fig. 4. Argand diagrams of our ρ and ω production amplitudes with nucleon helicity flip, at 6 and 17.2 GeV/c, for $-t$ = 0.1 and 0.3 GeV^2. For ease of comparison the 6 GeV/c amplitudes are scaled by the constant factor 6/17.2 ($\rho(\omega)$ production amplitudes are shown by solid (dotted) lines). Also shown are the magnitudes of the (incoherent) contributions ρ^+_{++}, A^+_{++}, Z^0_{++} and Z^-_{++}.

table 1. As shown in the Argand diagram of fig. 4, the cut C has its phase mainly antiparallel to B_- to achieve the required P_+/P_- ratio (ρ_{1-1} large and positive). A small contribution (C_ρ) antiparallel to ρ serves to swing the resultant of P_-^ω anticlockwise into better agreement with the $\rho-\omega$ interference phase data (sect. 3). One unpleasant feature is that $g_\rho/g_A \sim 2$, unlike the dual expectation of unity. This might be caused by normalization uncertainties in comparing the cross section for producing a wide resonance (ρ) with a narrow one (ω). However, in appendix A we discuss such normalization questions and no major uncertainty seems present.

A direct test of this exchange decomposition of ω production is in the energy dependence to higher energies and fig. 3 shows the 17 GeV/c prediction.

3. Polarization and interference effects in vector-meson production

The decomposition of the ρ and ω amplitudes discussed in sect. 2 is shown in the Argand diagrams of fig. 4. Characteristic features are the t and s depenence of the phase of P_{+-}^+ for ρ production, due to the interference between the cut C and A_2 contributions. The phase of C^ω is rather constant with energy and momentum transfer and influences the phases of $P_\pm$ for ω production as previously discussed. The non-flip nucleon couplings to Z, ρ and A_2 are also all significant and will give substantial polarization effects.

3.1. Interference effects

The relative phases of ρ and ω production amplitudes are observable from the electromagnetic $\rho-\omega$ mixing in the $\pi\pi$ decay channel and via SU(3) from a comparison of K* and $\overline{K^{*0}}$ production. The $\rho-\omega$ mixing in observable P_i (i.e. P_+, P_- or P_0) is controlled [20] by the bilinear combination of production amplitudes

$$P^i_{++}(\rho)P^i_{++}(\omega)^* + P^i_{+-}(\rho)P^i_{+-}(\omega)^*$$

$$= \xi_i[|P^i_{++}(\rho)|^2 + |P^i_{+-}(\rho)|^2]^{\frac{1}{2}}[|P^i_{++}(\omega)|^2 + |P^i_{+-}(\omega)|^2]^{\frac{1}{2}} e^{i\phi_i} . \qquad (3.1)$$

Thus the relative phase ϕ_i can be measured directly (with no ambiguities), while the coherence ξ_i can only be determined if the $\omega \to \pi\pi$ branching ratio is well known. The relation to K* production from SU(3) is

$$\sqrt{2}\,P^i(K^*) = P^i(\omega) + P^i(\rho) , \qquad \sqrt{2}\,P^i(\overline{K^*}) = P^i(\omega) - P^i(\rho) , \qquad (3.2)$$

where the phases are such that K* production would be real for exchange degenerate Regge poles in ρ and ω production. Thus for observables:

$$|P^i(K^*)|^2 - |P^i(\overline{K^*})|^2 = 2\mathrm{Re}[P^i_{++}(\rho)P^i_{++}(\omega)^* + P^i_{+-}(\rho)P^i_{+-}(\omega)^*]$$

$$= 2\xi_i[|P^i_{++}(\rho)|^2 + |P^i_{+-}(\rho)|^2]^{\frac{1}{2}}[|P^i_{++}(\omega)|^2 + |P^i_{+-}(\omega)|^2]^{\frac{1}{2}} \cos\phi_i . \qquad (3.3)$$

Table 2
$\rho-\omega$ interference phases

Amplitude	$-t$	6 GeV/c			17.2 GeV/c		
	(GeV^2)	ϕ (degree)	ξ	ϕ data (degree)	ϕ (degree)	ξ	ϕ data (degree)
	0–0.08	69	0.54	70 ± 30	69	0.43	
P_0	0.08–0.2	69	0.77		69	0.68	
	0.2 –0.45	69	0.81	45 ± 30	69	0.84	
	0–0.08	218	0.47		218	0.36	
P_-	0.08–0.2	106	0.38	70 ± 25	106	0.32	
	0.2 –0.45	87	0.71	120 ± 15	87	0.64	
	0–0.08	93	0.36	75 ± 30	180	0.19	
P_+	0.08–0.2	188	0.38	140 ± 20	241	0.64	205 ± 15
	0.2 –0.45	241	0.84	170 ± 20	255	0.95	230 ± 7

The phase (ϕ) and coherence (ξ) are defined in the text (eq. (3.1)). The preliminary data for ϕ is taken from refs. [14] (6 GeV/c) and [11] (17.2 GeV/c). The observed strength of $\rho-\omega$ interference effects in $\pi N \to \pi\pi N$ data is controlled by $\xi\Gamma(\omega \to \pi\pi)$. Compared to the usual assumption of complete coherence ($\xi = 1$), our predictions for ξ will result in values of $\Gamma(\omega \to \pi\pi)$ enhanced by $1/\xi$.

Thus the difference of K* and $\overline{\text{K}^*}$ observables yields similar information to $\rho-\omega$ interference, but uses the assumption of SU(3) and gives only $\xi_i \cos\phi_i$. The relative normalization of K* and $\overline{\text{K}^*}$ is also difficult to obtain with good precision experimentally. A comparison with preliminary $\rho-\omega$ interference and K* $-$ $\overline{\text{K}^*}$ data at 6 GeV/c [14] is presented in table 2 and fig. 5. The two types of data agree generally with each other and with the expectations of our models for ρ and ω production.

Since the $\omega \to \pi\pi$ branching ratio is not well determined, the coherence ξ has not been determined experimentally. The relative coherence, however, is found [14] to be smaller for P_+ than for P_- or P_0 and this is in general accord with our expectations. The change in phase with increasing $|t|$ of P^+_{++} for ρ production as the A_2 takes over from the cut combined with the relatively important P^+_{++} contributions yields a too-pronounced swing in $\rho-\omega$ interference phase for P_+. This feature can be improved by resorting to the solution (sect. 2) for ρ production with π^t_-/π^t_0 reduced and a consequent less steep t dependence of the cut and less dominant P^+_{++} contributions. The phase of $\lesssim 90°$ between the B and π exchange in P_0, and the phase of $\gtrsim 90°$ between ρ and ω production in P_- are well reproduced by our model amplitudes. A strong energy dependence of the $\rho-\omega$ phase for P_+ is also indicated in table 2.

The K* and $\overline{\text{K}^*}$ charge-exchange observables are in acceptable agreement except for P_-. Here, aside from a small effect due to $\frac{1}{3}\rho_{SS}$ present in the data, the effects of SU(3) breaking must be considered. This could be due to cuts which are not SU(3)

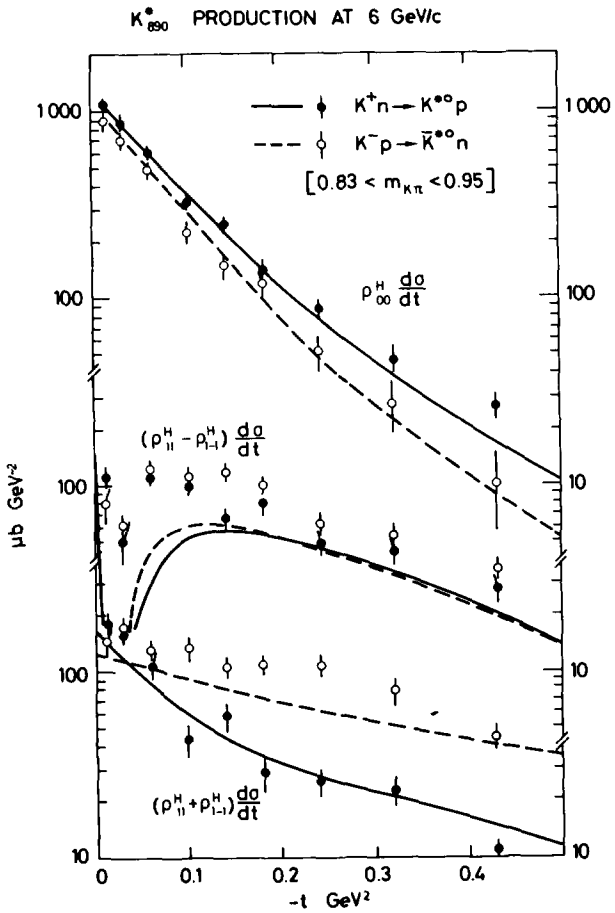

Fig. 5. Our SU(3) prediction and K* production data at 6 GeV/c ($\rho^{H}_{00}(d\sigma/dt)$, $(\rho^{H}_{11} \pm \rho^{H}_{1-1})$ $(d\sigma/dt)$). For the comparison with the preliminary data of ref. [14], which contains $\frac{1}{3}\rho_{SS}$ in each component and uses the mass cut ($0.83 < m_{K\pi} < 0.95$ GeV), the prediction has been multiplied by a factor 0.443.

octets in the t-channel – a serious possibility since the pomeron exchange is not empirically an SU(3) singlet and also Regge-Regge cuts can contribute. An alternative explanantion lies in SU(3) broken mass values which enter into the expression for the crossing matrix used to obtain the s-channel π exchange contributions to P_- from the t-channel expressions in which $\lambda_t = 0$ is dominant (eq. (2.2)). Thus for the vertex $a \to m$ by π exchange

$$\frac{\pi^s_-}{\pi^s_0} = \frac{2m\sqrt{-t'}}{m^2 + \mu^2 - a^2} . \tag{3.4}$$

This ratio is larger for $K \to K^*$ than for $\pi \to \rho$ processes. Thus in agreement with the data, a larger value of P_-/P_0 for $\overline{K^*}$ (or K^*) compared to ρ would be expected since the destructive interference of the cut enhances the effect beyond $t = -\mu^2$.

3.2. Polarization effects

Fig. 6 shows predictions for ρ and ω production polarization, as well as for $\gamma N \to \pi^+ N$ where vector dominance ($\gamma \sim \rho - \omega/2.8$) has been used. The polarization plotted, P_n, is that arising from natural parity exchange alone

$$P_n \sigma_n = -2\,\mathrm{Im}(P^+_{++} P^{+*}_{+-}), \qquad P\sigma = P_n \sigma_n + P_u \sigma_u . \tag{3.5}$$

In our model P_u is zero for ρ production and thus for ρ production and to a good approximation for photoproduction P_n can be equated with $P\sigma/\sigma_n$, which is the quantity plotted as data [21] in fig. 6. The structure in the polarization arises from the phase of P^+_{+-}, which swings from the phase of C^ρ to that of A_2 as $|t|$ increases and which thus passes through 90° relative to $P^+_{++} = A_{++}$ at an intermediate t-value. The energy dependence of P_N for $\pi N \to \rho N$ and $\gamma N \to \pi^+ N$ is also characteristic of our model with its significant $A_2 - C^\rho$ interference which shifts with energy.

P_u for ω production depends on the sign of the Z contribution which has not been determined. The effect of introducing an exchange degenerate A_1 contribution in $\pi N \to \rho n$ will be very small as argued previously and this is shown quantitatively for our choice of A_1–Z trajectory in table 3. Such small A_1/π ratios will not affect differential cross section and density matrix observables in which they enter quadratically, while polarization effects are linear in A_1/π and so could become significant at $|t| \sim 0.3$ or larger.

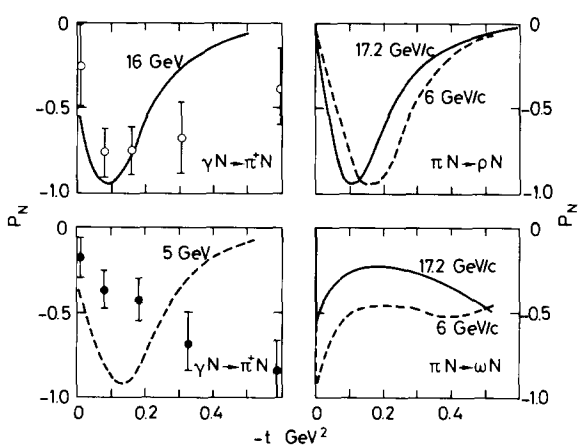

Fig. 6. Predicted nucleon polarization in vector meson production. The more reliably estimated natural parity exchange component (see eq. (3.5)) is shown. The prediction for $\gamma p \to \pi^+ n$ obtained from vector dominance is compared with data [21] at 5 and 16 GeV/c.

Table 3
The ratio of $Z(J^PI^G = 2^-1^+)$ to B exchange in helicity zero amplitudes at 17.2 GeV/c (as deduced from our model) and the exchange degeneracy prediction for the equivalent quantity A_1/π in ρ production

$-t$ (GeV^2)	$\lvert Z_0/B_0\rvert$	$\lvert A_{10}/\pi_0\rvert$
0.05	1.76	0.0094
0.1	1.24	0.023
0.3	0.67	0.112

Further polarized target observables can be measured [7] with the target polarization in the scattering plane. Quantities which are interference effects between natural and unnatural parity exchange can then be analysed. Thus the relative phase of P^0_{+-} and P^+_{++}, for instance, can be tested in $\pi N \to \rho N$. Such observables can be constructed from our parametrizations for the amplitudes and checked from the Argand diagrams of fig. 4.

4. Tensor meson production

4.1. Introduction

Spin-2 meson production on nucleons involves 10 helicity amplitudes which are related to density matrix elements and decay angular distribution moments as described in appendix A. The combinations which correspond to specific exchange naturality are

$$D^0_{\lambda\nu} = H^0_{\lambda\nu}, \qquad D^{1\pm}_{\lambda\nu} = \sqrt{\tfrac{1}{2}}(H^1_{\lambda\nu} \pm H^{-1}_{\lambda\nu}), \qquad D^{2\pm}_{\lambda\nu} = \sqrt{\tfrac{1}{2}}(H^2_{\lambda\nu} \mp H^{-2}_{\lambda\nu}). \quad (4.1)$$

D^{1+} and D^{2+} are the natural parity exchange amplitudes.

For spin-2 production, removing the spin 0 and 1 background in the decay channel is much more difficult than the analogous problem for spin-1 production. The presently available data on tensor meson production are also considerably less complete than for the vector production we have discussed. This leads us to try to combine our models for the exchange amplitudes in vector meson production with some additional theoretical input to describe the tensor meson amplitudes. This proves very useful as a preliminary study of tensor meson production.

Application of local duality to Regge + particle total cross sections [2] or to Regge + particle → particle + particle amplitudes [3] allows a general discussion of the relative production mechanisms for states of different mass but similar exchange quantum numbers. A much more specific analysis can be made by employing [4] the Regge recurrence production vertices in the dual resonance model. The latter

(dual boost model) yields specific expressions for the t dependence and helicity dependence of the Regge-pole exchange vertices for producing states on the same Regge trajectory (e.g. ρ–f–g or ω–A_2). We shall employ and investigate such dual model relations. The other necessary contribution, the cuts, will be deduced from the experimental data as far as possible.

4.2. $\pi N \to f^0 N$

The exchange contributions will be the same as those for $\pi N \to \rho N$ discussed in sect. 2 and we present here the "dual boost" predictions for f^0 production relative to ρ.

4.2.1. π exchange. At $t = \mu^2$ the coupling reduces to the relevant partial decay width to $\pi\pi$. The dual boost prediction of $\Gamma_f \sim 0.85\,\Gamma_\rho$ is smaller than the experimental [6] ratio $\Gamma_f \sim 1.03\,\Gamma_\rho$. However, the discrepancy is not serious – a factor of 1.1 in the production amplitude only. Our f^0 model is normalized to the experimental width as described in appendix A.

The $\lambda_t = 0, 1, 2$ or $\lambda_s = 0, 1, 2$ contributions from Reggeized π exchange have been calculated [4]. In the s-channel the helicity coupling ratios, normalized to 1 at $t = \mu^2$ for $\lambda_t = 0$, are given by

$$p_a^2 X_0^s = \tfrac{1}{4}[m^2 + 2\mu^2 + (t - \mu^2)(2 - 1/\alpha' m^2)] ,$$

$$p_a^2 X_{1-}^s = \tfrac{1}{2}\sqrt{-3t'}\,m ,$$

$$p_a^2 X_{2-}^s = -\tfrac{1}{2}\sqrt{3}\,t' , \qquad (4.2)$$

where $4p_a^2 = m^2 - 4\mu^2$ and m is the tensor meson mass. The t-dependence of f^0 production relative to ρ production is given by the dual vertex factor

$$\pi^i_{+-} = g^f_\pi X^s_i \frac{\sqrt{-t'}}{\mu^2 - t} e^{b_\pi t} e^{-\frac{1}{2} i\pi\alpha_\pi(t)} \left(\frac{p_L}{p_0}\right)^{\alpha_\pi(t)-1} . \qquad (4.3)$$

Compared to eq. (2.4), the only difference in t-dependence comes from the factor X_i^s. Thus for $\lambda_s = 0$, π^0_{+-} is a steeper function of t for f^0 production than for ρ production, since X_0^s is at small t equivalent to an exponential with slope 0.9 GeV^{-2}. This is a very clean prediction, characteristic of the dual vertex factor, since the more general dual approaches [2, 3] predict, on the contrary, an f^0 t-dependence less steep than for the ρ. These latter approaches are, however, less specific since they apply to the sum of all helicity contributions.

4.2.2. A_2 exchange. The ratio of natural parity exchange to unnatural parity exchange is expected to decrease with higher masses produced in all dual-based approaches [2, 4]. The specific "dual boost" model gives $g_A/g_\pi \sim 0.7$ of the ρ-produc-

tion ratio. The ratio of $\lambda_s = 2$ to $\lambda_s = 1$ is also specified:

$$\frac{A^{2+}_{+-}}{A^{1+}_{+-}} = \frac{2m\sqrt{-t'}}{m^2 + v^2 - \mu^2}, \tag{4.4}$$

where $\alpha_{A_2}(v^2) = 1$.

The t-dependence of A^{1+} is expected to be the same for f^0 as ρ production and the ratio r of ++ to +− nucleon couplings is also retained.

$$A^{1+}_{+-} = -g_A\, t' e^{b_A t}\, e^{-\frac{1}{2}i\pi\alpha_A(t)} \left(\frac{p_L}{p_0}\right)^{\alpha_A(t)-1}. \tag{4.5}$$

4.2.3. C exchange. In specific absorption models, the cut strength is tied to the π-pole strength and t dependence. Thus no substantial change from ρ to f^0 would have been expected. In practice, data show [6, 22] a reduction in g_c/g_π (at small t) of ~ 0.7 in going from the ρ to f^0. No explanation exists except for the possibility that some of the cut could come from A_2 absorption which would then decrease by such a factor as discussed above. Data analysis also indicates [12] the necessity of an $n = 1$ cut in the amplitude H^2_{+-} which vanishes like $\sqrt{-t'}$ instead of $(-t')^{\frac{3}{2}}$ as the pole contributions. Thus we choose a parametrization

$$C^{1+}_{+-} = C^{1-}_{+-} = g_C\, e^{b_C t}\, e^{-\frac{1}{2}i\pi\alpha_C(t)} \left(\frac{p_L}{p_0}\right)^{\alpha_C(t)-1},$$

$$C^{2+}_{+-} = C^{2-}_{+-} = \sqrt{-t'}\, g_{C_2}\, e^{b_C t}\, e^{-\frac{1}{2}i\pi\alpha_C(t)} \left(\frac{p_L}{p_0}\right)^{\alpha_C(t)-1}, \tag{4.6}$$

where $\alpha_C(t)$ is chosen the same as for ρ production.

4.2.4. Our model. In summary our exchange contribution are

$$D^0_{+-} = \pi^0_{+-},$$

$$D^{1-}_{+-} = \pi^{1-}_{+-} + C^{1-}_{+-}, \quad D^{1+}_{+-} = A^{1+}_{+-} + C^{1+}_{+-}, \quad D^{1+}_{++} = A^{1+}_{++},$$

$$D^{2-}_{+-} = \pi^{2-}_{+-} + C^{2-}_{+-}, \quad D^{2+}_{+-} = A^{2+}_{+-} + C^{2+}_{+-}, \quad D^{2+}_{++} = A^{2+}_{++}. \tag{4.7}$$

A complete separation of $J = 2$ effects from $J = 0$ and 1 in the f^0 region exists [12] at 17.2 GeV/c. This was achieved by parameterizing the f^0 production amplitudes and we show the result in fig. 7. Our dual boost plus ρ-production model approach is easily able to reproduce the amplitudes as shown in the figure. The parameters are given in table 1. In this description of f^0 amplitudes the π contributions were completely fixed as described above; the A_2 contributions were fixed except for g_A/g_π which is forced to be substantially smaller than the dual value; g_C, b_C and

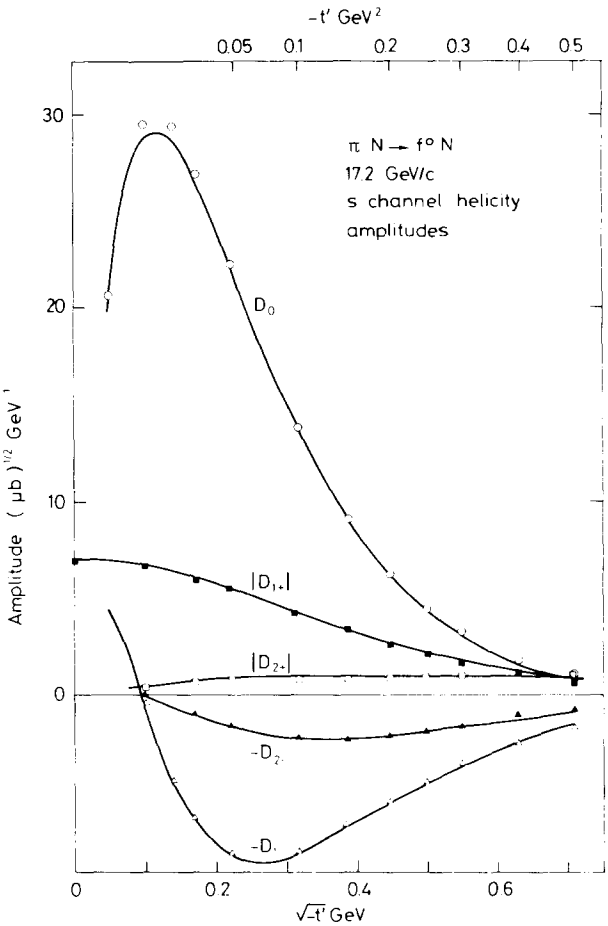

Fig. 7. The f^0 production amplitudes at 17.2 GeV/c. The points are the amplitudes as extracted in ref. [12] and the curves are our model reconstruction of them.

g_{C_2} were free and obtain reasonable values. Thus the dual vertex factors with little freedom reproduce the whole complex structure of the f^0 production amplitudes. In particular, D_0 is given entirely by the π contribution and the shrinkage of slope compared to ρ production is exactly predicted. The fraction of natural parity exchange in f^0 production is relatively small as predicted by the dual approaches and is consequently not well determined. We are thus unable to confirm the expected decrease in g_A/g_π from ρ to f of 0.7. Our f^0 production amplitudes are consistent with lower energy data. Such data exist either as bounds on $J = 2$ contributions [23] or with specific background assumptions [19] to separate out the f^0 component (see fig. 8).

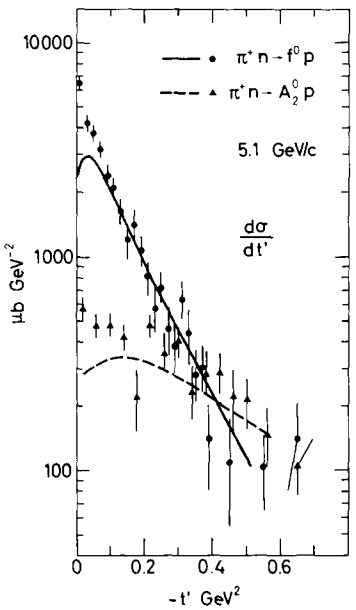

Fig. 8. f^0 and A_2 production differential cross sections at 5.1 GeV/*c*. The points are those of ref. [19] and the curve is the model prediction.

4.3. $\pi N \to A_2 N$ charge exchange

Available data on $\pi^- p \to A_2^0 n$ or $\pi^+ n \to A_2^0 p$ afford little help in constructing a model. A combination of exchange degeneracy relations applied to $\pi N \to f^0 N$, and dual boost relations applied to $\pi N \to \omega N$ give strong predictive power. The more so, since exchange degeneracy breaking has been investigated while comparing $\pi N \to \rho N$ with $\pi N \to \omega N$ and the dual boost relations have been tested in going from $\pi N \to \rho N$ to $\pi N \to f^0 N$. For the individual exchanges we assume the following.

4.3.1. B exchange. This is taken as exchange degenerate with the f^0 production π exchange contributions employing the same B/π ratio as eq. (2.9) with g_B/g_π fixed at the $\rho-\omega$ value.

4.3.2. ρ exchange. This is taken as exchange degenerate to the A_2 exchange amplitudes in f^0 production together with the factor $g_\rho/g_A = 2$ used in relating ρ to ω production (eq. (2.10)). Note that this factor of 2 largely compensates for the fact that the g_A/g_π ratio in f^0 production was much less than the dual boost value from ρ production. That the dual prediction persists is not unreasonable, since ρ exchange in $\pi \to A_2$ shares the same coupling as A_2 exchange in $\pi \to \rho$ when evaluated at the common A_2 pole and ρ pole.

4.3.3. Z exchange. The ratio of Z to B is as in eq. (2.12) with g_Z/g_B fixed at the ω production value (table 1) and B exchange as above.

4.3.4. Cut contributions. The effective cut in ω production $(C/g_B)_\omega$ is scaled by the same factor as the f^0 cut is in relation to the ρ cut:

$$(C/g_B)_{A_2} = (C/g_B)_\omega \, (g_C/g_\pi)_{f^0} \, (g_C/g_\pi)_\rho^{-1} \, . \tag{4.8}$$

The t dependence of the ω cut is already very flat, so that it is maintained unchanged for the A_2 production cut. In the same spirit, we also introduce an helicity 2 cut with the ratio of C_2/C the same as in f^0 production (g_{C_2}/g_C).

4.3.5. Our model. In summary, the exchange contributions are

$$D^0_{+-} = B^0_{+-} \, , \quad D^i_{+-} = B^i_{+-} + C^i_{+-} \, , \quad D^j_{+-} = \rho^j_{+-} + C^j_{+-} \, ,$$

$$D^0_{++} = Z^0_{++} \, , \quad D^i_{++} = Z^i_{++} \, , \qquad D^j_{++} = \rho^j_{++} \, , \tag{4.9}$$

where $i = 1-, 2-$ and $j = 1+, 2+$.

The model is completely specified in advance by a mixture of theoretical and phenomenological constraints. The predicted differential cross section for A_2 production is compared with some data at 5.1 GeV/c [19] in fig. 8 and the agreement is seen to be reasonable. Better data in the 3π or $\eta\pi$ decay mode, including density matrix elements or decay moments, would be of great interest in testing our ideas for the charge-exchange production of A_2.

Mearge evidence [24] on the energy dependence of $\pi^+ n \to A_2^0 p$ suggests a decrease of cross section with $\alpha_{\text{eff}} \sim 0$ consistent with the dominant unnatural exchange in our model.

Finally, in this section, we review the status of the dual boost factors which proved so useful in constructing tensor meson production amplitudes. In relating f^0 production to ρ production, the π exchange contribution is completely specified. The agreement is reasonable for the normalization (Γ_f/Γ_ρ), and excellent for the t-dependence of the $\lambda_s = 0$ amplitude $(b_\pi^f - b_\pi^\rho \sim 0.9 \text{ GeV}^{-2})$. The helicity structure proposed also avoids the problem of crossing matrix zeros in P_0 and D_0 and at the same time gives a satisfactory account of the measured helicity couplings on the exchange degenerate B-meson pole ($B \to \omega\pi$ dominantly $\lambda_\omega = 1$). The expected suppression of natural parity exchange relative to unnatural parity exchange in going from ρ to f_0 production is found in our analysis, but is stronger than anticipated. The same comparison between ω and A_2 production is closer to the expectation of the dual vertex model. A similar comparison of natural parity exchanges in data for $\pi N \to \rho N$ and $\pi N \to A_2 N$ with $I_t = 0$ also suggests [1] that they decrease somewhat more rapidly for the production of higher spin resonances than in the model.

5. Interference effects in f^0 and A_2 production

An Argand diagram of the f^0 and A_2 production amplitudes of our model at 17.2 GeV/c is shown in fig. 9. Compared to the $\rho-\omega$ situation (fig. 4) the most noticeable difference lies in D^f_{1+} which is dominated by the cut and so remains near 180° compared to D^ρ_{1+}. Thus (unlike ρ, ω production) the phase difference between f^0 and A_2 natural parity production amplitudes varies little with $-t$ ($\sim 120°$). The dominant unnatural parity-exchange amplitudes have a phase approximately 90° ahead for f production compared to A_2 production.

Just as for ρ and ω production, the relative phase between f^0 and A_2 production amplitudes is observable – and in two independent ways. The K*(1420) and $\overline{K^*}$(1420) charge-exchange production reactions are related by SU(3) to f^0 and A_2 analogously to eqs. (3.2) and (3.3). Fig. 10 shows the prediction of our model for the production cross-sections of these mesons compared with data [25, 26] near 4 GeV/c. Normalization uncertainties, particularly with a deuterium target, make this a rather imprecise test. Relatively well normalized data with density matrix element information would be needed to investigate the interference effects properly.

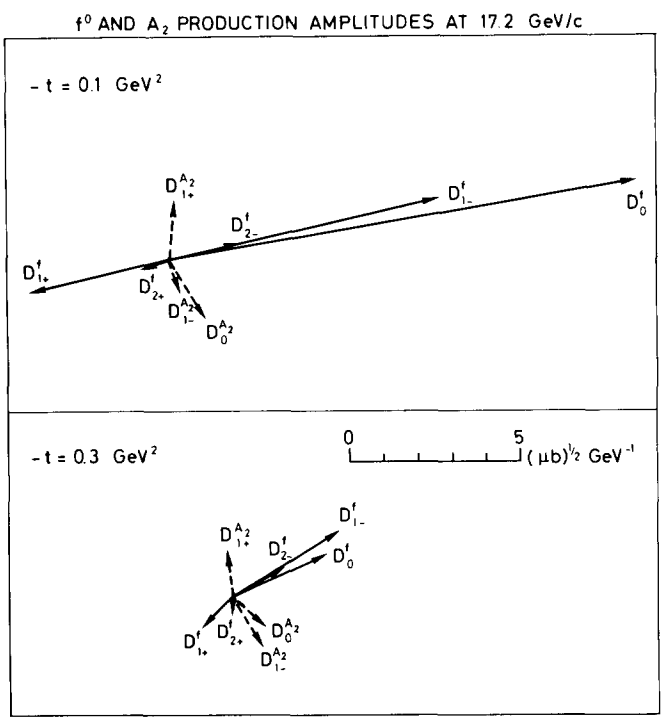

Fig. 9. Argand diagram of the model nucleon flip amplitudes for f^0 (solid lines) and A_2 (dotted) production at 17.2 GeV/c at $-t$ = 0.1 and 0.3 GeV^2. For clarity the (exceedingly small) amplitudes $D^{A_2}_{2\pm}$ are not shown.

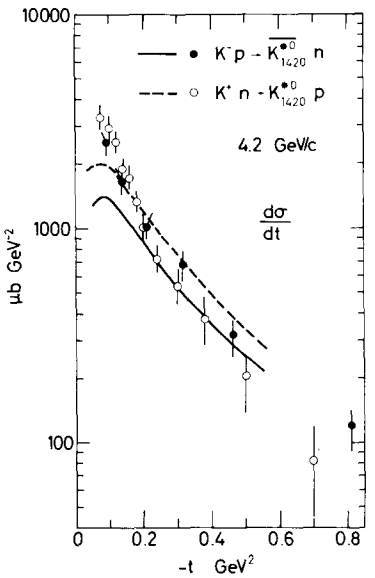

Fig. 10. Comparison of our SU(3) predictions for $K^-p \to \overline{K}^{*0}(1420)n$ (solid line) and $K^+n \to K^{*0}(1420)p$ (dotted line) with the 4.2 GeV/c data [25, 26] (solid and open points, respectively). The 4.6 GeV/c deuterium data of ref. [26] has been scaled by $(4.2/4.6)^{-2}$ to an effective momentum of 4.2 GeV/c.

A more complete test in principle, analogous to ρ–ω interference, is provided [27] by the common decay channel of f^0 and A_2 into $K\bar{K}$. Both mesons can decay by strong interactions with comparable strength into $K^0\bar{K}^0$ and K^+K^- and interferences between their combined production and decay amplitudes will result. Generalizing eqs. (A.3)–(A.7) of appendix A this gives observable combinations of the form

$$\sum_{\mu} |F^i_\mu(s,t)\, B^f(m) + A^i_\mu(s,t)\, B^{A_2}(m)|^2 , \tag{5.1}$$

where F^i_μ and A^i_μ ($i = 0, 1\pm, 2\pm$) represent production amplitudes (assumed approximately constant in $K\bar{K}$ invariant mass m) and B^f and B^{A_2} are the decay factors of eq. (A.5). The phase and modulus of these decay factors are illustrated in fig. 11. The mass, width and branching ratio parameters used are collected in appendix B. The relative phase $\delta_f - \delta_{A_2}$ of the f^0 and A_2 resonance decay factors is also shown as a function of $K\bar{K}$ mass in fig. 11. This is of interest since it is the variation of this phase with m that allows the ambiguity in the sign of the relative f and A_2 production phase to be resolved. Thus, like ρ–ω interference, a more complete measurement is possible in principle and with no SU(3) assumptions. The relevance of the relative phase depending on m is understood on considering the interference term in eq. (5.1):

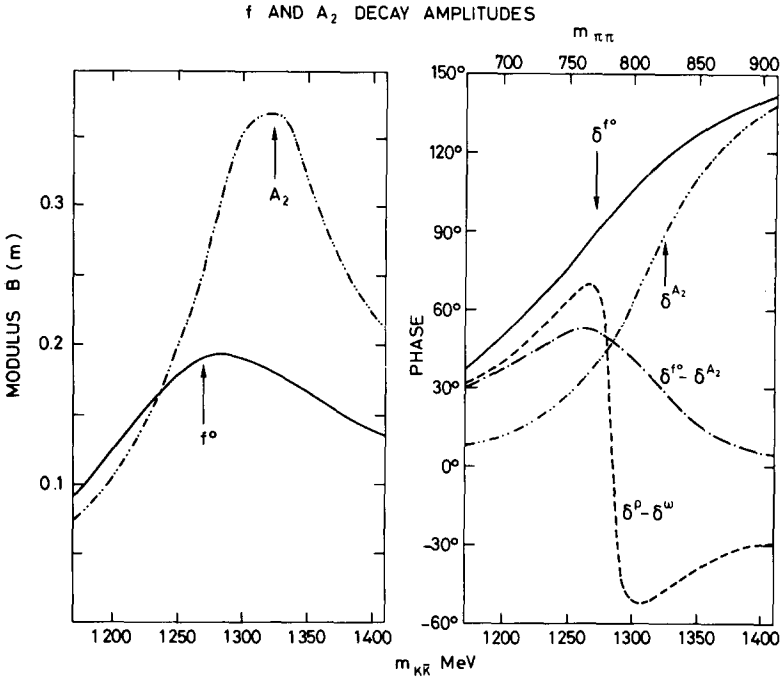

Fig. 11. The modulus and phase of the $f^0 \to K^+K^-$ (full curve) and $A_2 \to K^+K^-$ (double-dotted curve) Breit-Wigner decay amplitudes $B(m_{K\bar{K}})$ [eq. (A.5)]. The mass, width and branching ratios used are discussed in appendix B. We also compare the resonance phase differences $\delta^{f}-\delta^{A_2}$ (single-dotted curve) and $\delta^{\rho}-\delta^{\omega}$ (dashed) where the mass scales are chosen to coincide at $m_{K\bar{K}} = 1270$, $m_{\pi\pi} = 770$ MeV ($(m, \Gamma)_{\rho} = (772, 143)$; $(m, \Gamma)_{\omega} = (784, 10)$ MeV).

$$\sum_{\mu} \mathrm{Re}(F^i_{\mu} A^{i*}_{\mu} B^{f}(m) B^{A_2}(m)^*)$$
$$= \xi_i \{\sum_{\mu} |F^i_{\mu}|^2\}^{\frac{1}{2}} \{\sum_{\mu} |A^i_{\mu}|^2\}^{\frac{1}{2}} |B^{f}(m)|\, |B^{A_2}(m)| \cos(\phi_i + \delta_f(m) - \delta_{A_2}(m)). \quad (5.2)$$

The known m variation of B and thus δ then allows the $f-A_2$ relative production phase ϕ_i to be uniquely determined.

In practice this effect can be well controlled since, because of isospin, the f^0-A_2 interference changes sign both with the change from proton to neutron target (as for $\rho-\omega$ interference) and with the change from K^+K^- to $K^0\bar{K}^0$ decay channel. An easy way to visualize the respective signs for the four relevant processes is via duality diagrams as shown in fig. 12. Thus processes (b) and (c) $\pi^-p \to K^-K^+n$ and $\pi^+n \to K^0\bar{K}^0p$ have real production phase duality diagrams (like $KN \to K^*(1420)N$) while (a) and (d), $\pi^-p \to K^0\bar{K}^0n$ and $\pi^+n \to K^+K^-p$, have rotating phase (like $\bar{K}N \to \bar{K}^*(1420)N$). Thus for processes (b) or (c) the production phases will be as drawn for the Argand diagram of fig. 9, while for (a) or (d) an extra 180° is needed.

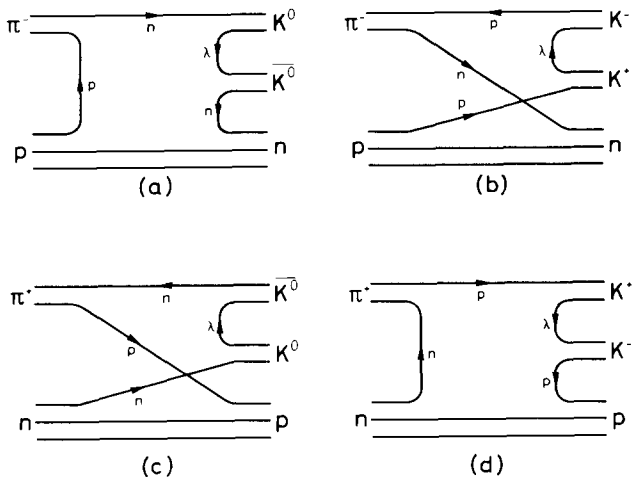

Fig. 12. Duality diagrams for the four processes: (a) $\pi^- p \to K^0 \bar{K}^0 n$, (b) $\pi^- p \to K^- K^+ n$, (c) $\pi^+ n \to K^0 \bar{K}^0 p$ and (d) $\pi^+ n \to K^+ K^- p$.

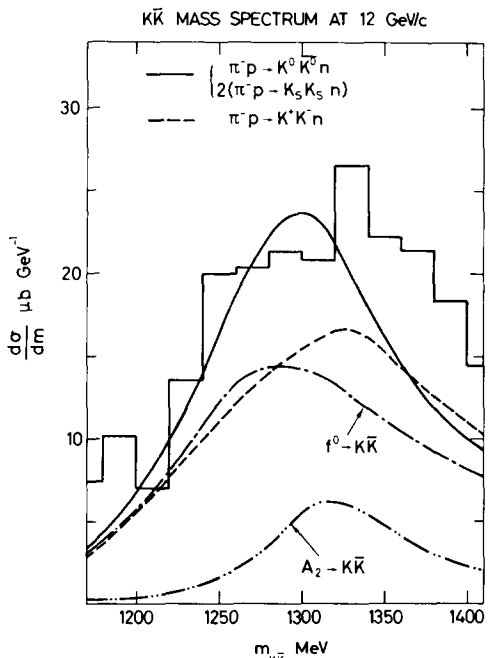

Fig. 13. The predicted $K\bar{K}$ mass spectrum ($|t| < 0.5$ GeV^2) for $\pi^- p \to K^+ K^- n$ and $\pi^- p \to K^0 \bar{K}^0 n$ at 12 GeV/c is compared with the $\pi^- p \to K^0_S K^0_S n$ data of ref. [29].

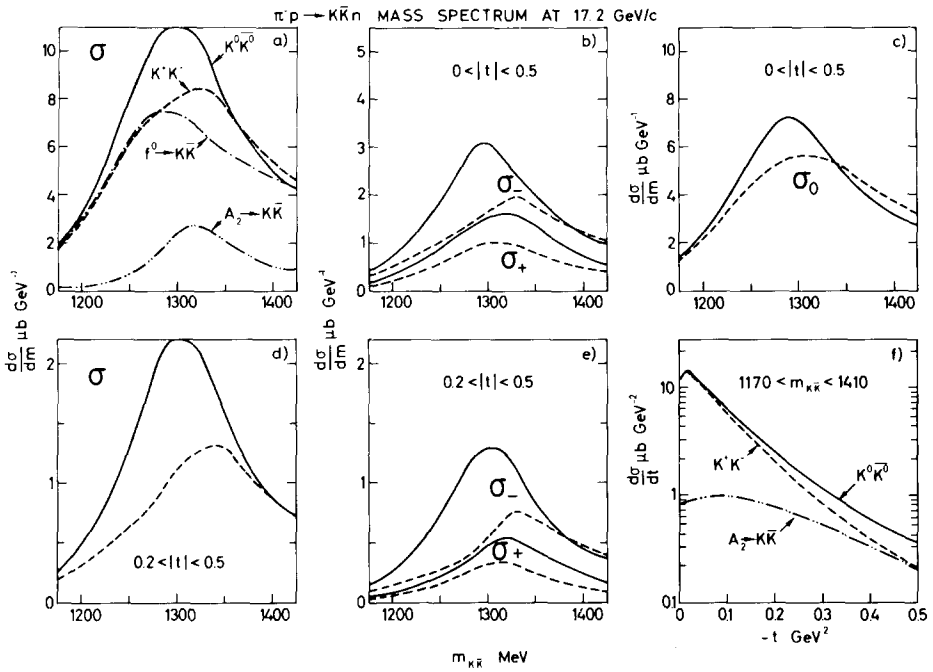

Fig. 14. The predicted mass spectrum $d\sigma/dm$ of $\pi^- p \to K\bar{K}n$ at 17.2 GeV/c integrated over $|t| < 0.5$ GeV^2 ((a) (b) and (c)) and over $0.2 < |t| < 0.5$ GeV^2 ((d) and (e)). (a) and (d) show σ, the full mass spectrum; (c) shows the helicity zero contribution σ_0; and the helicity one and two contributions are given by their natural (σ_+) and unnatural (σ_-) parity contributions in (b) and (e). (f) shows $d\sigma/dt$ integrated over the region $1170 < m_{K\bar{K}} < 1410$ MeV as a function of t. The $\pi^- p \to K^0\bar{K}^0 n$ (K^+K^-n) predictions are shown by full (dashed) curves. Contributions proceeding via f^0 (A_2) production are shown by single- (double-) dotted curves.

As an example, consider the contribution to $|D_0|^2$. At $m \sim m_{f^0}$ the f^0 Breit-Wigner phase is $\sim 50°$ ahead of the A_2 resonance decay phase (see fig. 11) and the f^0 production amplitude is $\sim 70°$ ahead of the A_2 production (see fig. 9) so that the overall relative phase will be $\sim 120°$ (destructive) for (b) or (c) and $\sim 120° + 180°$ (constructive) for reactions (a) or (d).

More comprehensive predictions are shown in figs. 13, 14 and table 4 for different combinations of observables in $\pi N \to K\bar{K}N$. Fig. 14 shows the various components of $d\sigma/dm$ for $|t|$ cuts of $0 < |t| < 0.5$ and for $0.2 < |t| < 0.5$ GeV^2. The latter cut samples the region of largest production phase difference in D_{1-} so exhibiting larger interference effects in $d\sigma_-/dm$ and hence in $d\sigma/dm$ ($d\sigma_+/dm$ is small and the helicity zero production phase difference is independent of t in our model). A general feature of the predicted mass spectra of figs. 13 and 14 is that the maxima of both $\pi^- p \to K^- K^+ n$ and $\pi^- p \to K^0\bar{K}^0 n$ are shifted from the position of the dominant f^0 (1270 MeV) towards higher masses (to 1325 and 1300 MeV, respectively).

Table 4
The predicted normalized moments of the $K\bar{K}$ angular distribution in $\pi^- p \to K\bar{K}n$ at 17.2 GeV/c and $m_{K\bar{K}} = 1310$ MeV ($\langle Y_0^0 \rangle = 1/\sqrt{4\pi}$)

Moment	$K^0\bar{K}^0$	K^+K^-
$\langle Y_0^2 \rangle$	0.132	0.140
$\langle Y_2^2 \rangle$	−0.010	−0.009
$\langle Y_0^4 \rangle$	0.089	0.118
$\langle Y_1^4 \rangle$	0.081	0.082
$\langle Y_1^2 \rangle$	0.062	0.051
$\langle Y_2^4 \rangle$	0.032	0.030
$\langle Y_3^4 \rangle$	0.011	0.013
$\langle Y_4^4 \rangle$	0.002	0.001

For $\pi^- p \to K^- K^+ n$ (or equivalently $\pi^+ n \to K^0 \bar{K}^0 p$) the shift is more marked and a definite asymmetry around 1325 MeV is anticipated.

Also shown in fig. 14 is $d\sigma/dt$ (in the mass region $1.17 < m < 1.41$ GeV) for $\pi^- p \to K^+ K^- n$ and $\pi^- p \to K^0 \bar{K}^0 n$. The interference effects are seen to be small. Another way to exhibit the data is to show the normalized moments $\langle Y_M^L \rangle$ (eq. (A.6)) for $K\bar{K}$ production. However, these are predicted to have very weak m dependence and small interference effects. This is understandable since in general each $\langle Y_M^L \rangle$ is a sum over many exchange components whose contributions tend to be diluted. In table 4 we give the predicted values of the $\langle Y_M^L \rangle$ at $m = 1310$ MeV, where the $K\bar{K}$ spectra are approximately maximal. Only the $\langle Y_M^4 \rangle$ moments will be independent of S- and P-wave background uncertainties.

To make maximum use of interference effects, care of these $J < 2$ contributions and of accurate relative normalization will be needed experimentally. Another source of uncertainty is the precise $f^0 \to K\bar{K}$ (and to a lesser extent $A_2 \to K\bar{K}$) branching ratio. The quoted [28] value of $f^0 \to K\bar{K}/f^0 \to \text{all} = 0.05 \pm 0.03$ is based on data samples in which the effects of $f^0 - A_2$ interference have had to be taken into account in principle. Thus, since we have a reasonable model for the relative strength and phase of f^0 and A_2 production in $\pi N \to K\bar{K}N$, we are in a position to re-evaluate the $f^0 \to K\bar{K}$ branching ratio. As an example, fig. 13 shows data [29] on $\pi^- p \to K^0 \bar{K}^0 n$ at 12 GeV/c, together with our (absolute) prediction* including $f^0 - A_2$ interference and using $f^0 \to K\bar{K}/f^0 \to \text{all} = 0.025$. Taking account of the normalization error on the data, and the possible contribution of S- and P-wave $K\bar{K}$; this yields a $K\bar{K}$/all branching ratio 0.025 ± 0.01. Our curves in fig. 14 are evaluated with this branching ratio which has the virtue of being closer to the theoretical

* This contrasts with the experimental analysis [29] of the same data which added incoherently f^0 and A_2 and, estimating equal contributions of the two resonances, compared with the then existing f^0 production data in the $\pi\pi$ mode and claimed $f^0 \to K\bar{K}/f^0 \to \pi\pi \sim 0.05$.

value from SU(3). Thus, ideal mixing in the tensor meson nonet gives equal $f^0K\bar{K}$ and $A_2K\bar{K}$ couplings and allowing for D-wave phase space $\Gamma_{f^0K\bar{K}} = 0.7$ $\Gamma_{A_2K\bar{K}} \sim 3.4$ MeV, i.e. $\Gamma(f^0 \to K\bar{K})/\Gamma(f^0 \to \text{all}) \sim 0.02$.

6. Conclusions

(i) The simple exchange-model ideas of exchange-degenerate, factorizing, SU(3) symmetric t-channel Regge poles, together with empirical cuts in over-all non-flip amplitudes, have proved a very useful guide to the data. Exchange-degeneracy breakings of up to factors of 2 have been found necessary, in particular between ρ and A_2 exchanges in vector meson production. It is important to consider *a priori* all allowed pole exchanges (i.e. B, A_1, Z ...) and then argue why their contributions might be negligible (as for A_1 exchange in $\pi N \to \rho N$).

(ii) The dual boost factors provide an economical description of higher spin meson production. The predicted mass/spin dependence of the natural/unnatural pole couplings, meson vertex helicity couplings and production t dependences proved very satisfactory in the case of ρ and f^0 production. The dual vertex helicity couplings were also shown to describe well the dominantly $\lambda_\omega = 1$ decay $B \to \omega\pi$.

(iii) The empirically determined cut in ρ production has a remarkably steep t dependence, although this can be alleviated by modifying the π^t_-/π^t_0 ratio. For f^0 production the cut is relatively smaller at $t = 0$ and is less steep. No convincing theoretical explanation exists, although one possible contributory factor was discussed.

(iv) Improved data on the charge-exchange production of ω, A_2 and f^0 over a range of energies will allow many of the above feature to be clarified. Together with polarization data, or data on the $K\bar{K}$ decay of $f^0 - A_2$ (predictions for which were presented), many more model-independent lines of analysis become accessible. Our preliminary study of tensor meson production can easily be extended to higher spin mesons – for instance the spin-3 states g and $\omega^*(3^-)$. Thus the systematics of the dependence of the production amplitudes on the external mass and spin can be established as soon as the relevant data becomes available.

(v) Our preliminary analysis of $f^0 - A_2$ interference in $\pi N \to K\bar{K}N$ (in which the important role of the production amplitudes is emphasized) allows an estimate to be made of the $f^0 \to K\bar{K}/f^0 \to$ all branching ratio which we find to be 0.025 ± 0.010.

We are grateful to Alan Martin and Penny Estabrooks for helpful discussions and communications.

Appendix A. Normalization and spin

Consider the process $a + b \to m + e$, where m is a spin-J resonance of helicity λ which decays with invariant mass m into two spinless particles c and d. In the rest

frame of m, the direction of $\boldsymbol{p}_c$ is described by spherical polar angles θ and ϕ in a frame with Oy normal to the scattering plane and Oz either along $\boldsymbol{p}_a$ in the t-channel frame or along $-\boldsymbol{p}_e$ in the s-channel frame. The helicity amplitude for a + b → c + d + e can be factorized into a production amplitude A^J and a decay matrix element M^J

$$A^{\mu_a}_{\mu_e\mu_b}(s,t,m^2,\theta,\phi) = \sum_\lambda A^{J\lambda\mu_a}_{\mu_e\mu_b}(s,t,m^2)\frac{M^J\, \mathrm{d}^J_{\lambda 0}(\cos\theta)\mathrm{e}^{i\lambda\phi}}{m_J^2 - m^2 - im\Gamma_T(m)}, \tag{A.1}$$

where

$$|M^J|^2 = \frac{8\pi m}{q}(2J+1)\, m_J \Gamma_{cd}(m)\,. \tag{A.2}$$

We normalize A such that the differential cross section

$$\frac{\mathrm{d}\sigma}{\mathrm{d}t\,\mathrm{d}m^2\mathrm{d}\Omega} = \frac{1}{(2\pi)^3}\overline{\sum_\mu}\frac{q_{cd}}{4m}|A^{\mu_a}_{\mu_c\mu_b}(s,t,m^2,\theta,\phi)|^2\,, \tag{A.3}$$

where an average over initial spin states and sum over final spin states is implied.

Integrating over the decay angular distribution exhibited in eq. (A.1)

$$\frac{\mathrm{d}\sigma}{\mathrm{d}t\,\mathrm{d}m^2} = \overline{\sum_{\mu,\lambda}}|A^{J\lambda\mu_a}_{\mu_c\mu_b}(s,t,m^2)B^J(m)|^2\,, \tag{A.4}$$

where

$$B^J(m) = \frac{[m_J\Gamma_{cd}(m)/\pi]^{\frac{1}{2}}}{m_J^2 - m^2 - im\Gamma_T(m)} \tag{A.5}$$

are the decay factors relevant.

The generalization to the expectation value of the angular decay moments $Y^L_M(\theta,\phi)$ gives

$$\langle Y^L_M\rangle = \frac{1}{\sqrt{4\pi}}\sum_{\lambda,\lambda'}\frac{2J+1}{\sqrt{2L+1}}\langle JJ00|L0\rangle(-1)^{\lambda'}\langle J\lambda{-}\lambda'|LM\rangle\rho^J_{\lambda\lambda'}\,, \tag{A.6}$$

with

$$\rho^J_{\lambda\lambda'}(m^2)\frac{\mathrm{d}\sigma}{\mathrm{d}t\,\mathrm{d}m^2} = \overline{\sum_\mu}\,\mathrm{Re}[A^{J\lambda\mu_a}_{\mu_e\mu_b}(s,t,m^2)B^J(m)A^{J\lambda'\mu_a}_{\mu_e\mu_b}(s,t,m^2)^*\,B^J(m)^*]\,. \tag{A.7}$$

For resonance production it is convenient to introduce production amplitudes averaged over the resonance mass spectrum and corrected for all decay modes. Thus

the natural definition of a production cross section is to integrate over the resonance peak:

$$\frac{\mathrm{d}\sigma}{\mathrm{d}t} = \frac{\Gamma_T}{\Gamma_{cd}} \int_{m_L^2}^{m_H^2} \mathrm{d}m^2 \frac{\mathrm{d}\sigma}{\mathrm{d}t\,\mathrm{d}m^2}$$

$$= \frac{I(m_L^2, m_H^2)}{(2s_a+1)(2s_b+1)} \sum_{\mu,\lambda} |A^{J\lambda\mu_a}_{\mu_e\mu_b}(s,t,m_J^2)|^2 , \qquad \text{(A.8)}$$

which introduces the average production amplitudes. The average I is defined so that it is unity for a narrow resonance. In general, it depends on the mass dependence of the production amplitudes A^J and the decay factors B^J:

$$I(m_L^2, m_H^2) = \frac{\Gamma_T}{\Gamma_{cd}} \int_{m_L^2}^{m_H^2} \mathrm{d}m^2 |B^J(m)|^2 \sum_{\mu,\lambda} |A^J(m^2)|^2 / \sum_{\mu,\lambda} |A^J(m_J^2)|^2 . \qquad \text{(A.9)}$$

Analogous averaged results hold for the moments and density matrix elements of resonance production. For explicit expressions and an extension to a mixture of spin states see ref. [23].

In the special case of π exchange at $t = \mu^2$, however, the dependence of the production amplitude on m^2 is known and can be used to obtain the normalization of ρ and f^0 production. Thus A^J contains [6] an additional factor of M^J controlling the production of resonance J by π exchange. Thus

$$I_\pi = \frac{1}{\pi} \frac{\Gamma_T(m_J)}{\Gamma_{cd}(m_J)} \int_{m_L^2}^{m_H^2} \mathrm{d}m^2 \frac{m_J \Gamma_{cd}(m^2)}{|m_J^2 - m^2 - im\Gamma_T(m^2)|^2} \frac{q_J m}{m_J q} \frac{\Gamma_{cd}(m^2)}{\Gamma_{cd}(m_J^2)} . \qquad \text{(A.10)}$$

This, combined with the Chew-Low formula [6], enables the production cross section at $t \to \mu^2$ to be normalized

$$\frac{(t-\mu^2)^2}{-t'} \frac{\mathrm{d}\sigma}{\mathrm{d}t}\bigg|_{t=\mu^2} = \frac{2\pi}{m_N^2 p_L^2} \frac{g^2}{4\pi} C_I (2J+1) m_J \Gamma_{cd}(m_J) I_\pi . \qquad \text{(A.11)}$$

The right-hand side at $p_L = 17.2$ GeV/c, with $g^2/4\pi = 14.4$, taking $I_\pi = 1$, has a value $(6.55)^2$ μb for ρ production ($I = 1$; $c_I = 1$; $\Gamma(m_J) = 0.143$) and a value of $(9.2)^2$ for f^0 production ($I = 0$; $c_I = \frac{2}{3}$; $\Gamma_{\pi\pi}(m_J) = 0.81 \times 0.182$). These values are used for normalizing our production amplitudes by equating them to $g_\pi^2 e^{2b_\pi \mu^2}$ (see table 1). Representative values of $I_\pi(m_L^2, m_H^2)$ calculated from the $\pi\pi$ phase shifts [6] are

$$I_\pi^\rho(0.490, 0.689) = 0.495 , \qquad I_\pi^\rho(0.078, 1.562) = 1.028 .$$

Thus about $\pm 3\Gamma$ in m is needed to have $I_\pi^\rho \sim 1$. For the f^0, with $\pm 3\Gamma$ mass range

$I_\pi^f = 0.96$. Thus our normalization of the ρ and f production amplitudes corresponds in practice to taking a mass range of $\pm 3\Gamma$. For the ω, which is very narrow, our prescription depends less on the production amplitude and is equivalent to taking the whole signal – to which $\pm 3\Gamma$ is a good approximation.

Appendix B. Decay amplitudes for f^0 and A_2

To evaluate the resonance decay factors $B(m)$ (eq. (A.5) of Appendix A) we need the dependence of the total width Γ_T and partial width Γ_{cd} on subenergy m. For a D-wave resonance it is customary to use a centrifugal barrier factor

$$\Gamma(m) = \left(\frac{q}{q_R}\right)^5 \Gamma(m_R) \frac{D_2(q_R R)}{D_2(qR)},$$

where $D_2(x) = 9 + 3x^2 + x^4$, q is the decay momentum into the relevant channel, and R is a constant representing the radius of interaction.

For the f^0 we take [6] (in GeV units): $m_f = 1.27$, mass dependence of Γ_T from $\Gamma_T(m_f) = 0.182$, $R = 3.5$ with q as $\pi\pi$ decay momentum; mass dependence of $\Gamma_{K\bar{K}}$ from $\Gamma_{K\bar{K}}(m_f)/\Gamma_T = 0.025$ (see text), $R = 3.5$ with q as $K\bar{K}$ decay momentum.

For the A_2 we take [30] $m_{A_2} = 1.324$; mass dependence of Γ_T from $\Gamma_T(m_{A_2}) = 0.104$, $R = 3.5$ with q as a $\pi\rho$ decay momentum; mass dependence of $\Gamma_{K\bar{K}}$ from $\Gamma_{K\bar{K}}(m_{A_2})/\Gamma_T = 0.06$ [31], $R = 3.5$ with q as $K\bar{K}$ decay momentum.

References

[1] C. Michael, Proc. 16th Int. Conf. on high-energy physics, Chicago-Batavia, 1972 (NAL, Batavia, Ill., 1973) vol. 3, p. 165;
R. Diebold, Proc. 2nd Int. Conf. on elementary particles, Aix-en-Provence, 1973, J. de Phys. Suppl. 34 Cl-1973, p. 284.
[2] P. Hoyer, R.G. Roberts and D.P. Roy, Nucl. Phys. B56 (1973) 173.
[3] P. Hoyer and J. Kwiecinski, Nucl. Phys. B60 (1973) 26.
[4] C. Michael, Nucl. Phys. B63 (1973) 431.
[5] P. Estabrooks and A.D. Martin, Phys. Letters 41B (1972) 350.
[6] P. Estabrooks et al., Proc. AIP Conf. on particles and fields, Tallahassee, 1973 (AIP, New York, 1973) p. 37.
[7] G.C. Fox, Proc. 2nd Int. Conf. on polarization and polarized targets, Berkely, 1971, Caltech. preprint CALT-63-334 (1971);
J.D. Kimel and E. Reya, Nucl. Phys. B58 (1973) 513.
[8] C. Michael, Springer Tracts in modern physics, ed. G. Höhler, (Springer Verlag, Berlin, 1970) vol. 55, p. 174.
[9] H. Pilkuhn et al., Nucl. Phys. B65 (1973) 460.
[10] G.L. Kane and M. Ross, Phys. Rev. 177, (1969) 2353;
C.D. Froggatt and D. Morgan, Phys. Rev. 187 (1969) 2044;
G.C. Fox, Proc. Conf. on phenomenology in particles physics, Pasadena, 1971 (Cal. Inst. Tech., Pasadena, Calif., 1971), p. 703.

[11] P. Estabrooks, A.D. Martin and C. Michael, Nucl. Phys. B72 (1974) 454.
[12] A.D. Martin, Proc. 4th Int. Symp. on multiparticle hadrodynamics, Pavia, 1973; CERN TH. 1741.
[13] G. Grayer et al., Proc. 4th Int. Conf. on high-energy collisions, Oxford, 1972 (Rutherford High Energy Laboratory, Chilton, Didcot, Berks., 1972), RHEL-72-001, vol. 2, p. 26.
[14] D.S. Ayres, Proc. AIP Conf. on particles and fields, Tallahassee, 1973 (AIP, New York, 1973) p. 302;
R. Diebold, quoted in ref. [1] and private communication.
[15] R.D. Field and D.P. Sidhu, Phys. Rev. D10 (1974) 89;
M. Ross, F.S. Henyey and G.L. Kane, Nucl. Phys. B23 (1970) 269.
[16] S.U. Chung et al., Phys. Letters 47 B (1973) 526;
V. Chaloupka, Proc. 2nd Int. Conf. on elementary particles, Aix-en-Provence, 1973, J. de Phys. Suppl., 34 11-12 Cl-1973, p. 213; CERN preprint D.Ph. II/Phys. 73–33 (1973).
[17] F. Gilman, M. Kugler and S. Meshkov, SLAC Pub. 1235 (1973).
[18] J.C. Anderson et al., Phys. Letters B45 (1973) 165;
L.E. Holloway et al., Phys. Rev. D8 (1973) 2814;
J.A. Mathews et al., Phys. Rev. Letters 26 (1971) 400.
[19] N. Armenise et al., Nuovo Cimento 65A (1970) 637.
[20] A.S. Goldhaber, G.C. Fox and C. Quigg, Phys. Letters 30B (1969) 249.
[21] G.C. Morehouse et al., Phys. Rev. Letters 25 (1970) 835;
D.J. Sherden et al., Phys. Rev. Letters 30 (1973) 1230;
C. Geweniger et al., Phys. Letters 29B (1969) 41;
H. Burfeindt et al., Phys. Letters 33B (1970) 509.
[22] W. Ochs and F. Wagner, Phys. Letters 44B (1973) 2[illegible].
[23] J.A. Charlesworth et al., Nucl. Phys. B65 (1973) 253.
[24] J.T. Carroll et al., Phys. Rev. Letters 25 (1970) 1393.
[25] M. Aguilar-Benitez et al., Phys. Rev. D4 (1971) 2858.
[26] K. Buchner et al., Nucl. Phys. B45 (1972) 333.
[27] C. Michael and V. Ruuskanen, Phys. Letters 35B (1971) 47;
J. Rosner, Proc. Conf. on phenomenology in particle physics, Pasadena, 1971 (Cal. Inst. Tech., Pasadena, Calif., 1971) p. 387.
[28] Particle Data Group, Rev. Mod. Phys. 45 No. 2, Part II (1973).
[29] W. Beusch et al., Phys. Letters 25B (1967) 357.
[30] G. Conforto et al., Phys. Letters 45B (1973) 154.
[31] V. Chaloupka et al., Phys. Letters 44B (1973) 211.